Published in final edited form as:
Trends Biotechnol. 2011 May ; 29(5): 213–221. doi:10.1016/j.tibtech.2011.01.006.

Photoacoustic imaging in cancer detection, diagnosis, and treatment guidance

Srivalleesha Mallidi, **Geoffrey P. Luke**, and **Stanislav Emelianov**
Department of Biomedical Engineering, University of Texas at Austin, Austin, TX 78712, USA

Abstract

Imaging modalities play an important role in the clinical management of cancer, including screening, diagnosis, treatment planning, and therapy monitoring. Owing to increased research efforts in the past two decades, photoacoustic imaging – a non-ionizing, non-invasive technique capable of visualizing optical absorption properties of tissue at reasonable depth, with spatial resolution of ultrasound – has emerged. Ultrasound-guided photoacoustics is regarded for its ability to provide *in vivo* morphological and functional information about the tumor within the surrounding tissue. With the recent advent of targeted contrast agents, photoacoustics is capable of *in vivo* molecular imaging, thus facilitating further molecular and cellular characterization of cancer. This review examines the role of photoacoustics and photoacoustic-augmented imaging techniques in comprehensive cancer detection, diagnosis and treatment guidance.

Introduction

Cancer is a vicious disease that killed approximately 570,000 people in 2010 in the United States alone [1]. To develop successful therapeutic strategies and prevent recurrence of the disease, structural, functional and metabolic properties of this disease need to be well-characterized. The research efforts are not only limited to developing new treatments and discovering the root cause for the disease, but also in developing imaging technologies that can aid in early detection of cancer and can provide comprehensive real-time information on the tumor properties. Currently, ultrasound imaging (USI), magnetic resonance imaging (MRI), X-ray computed tomography (CT), and nuclear imaging techniques like positron emission tomography (PET) and single photon emission computed tomography (SPECT) are being used to detect tumors in patients [2]. With the development of various targeted contrast agents, these imaging techniques are also able to provide molecular information of the malignant tumor tissue. However, microscopic optical imaging techniques have higher resolution (~0.1–100 μm) than USI (50–500 μm), MRI (10–100μm), CT (50–200 μm), PET (1–2 mm) and SPECT (1–2 mm), and can detect a lower number of cancer cells per imaging voxel [3]. Traditional diffusive regime optical imaging techniques, such as diffuse optical tomography (DOT), have high detection sensitivity; however, the resolution is limited to ~5 mm. The need for an imaging technique that can provide high optical contrast images at microscale resolution and at a reasonable penetration depth has now been filled with photoacoustic imaging (PAI).

Corresponding author: Emelianov, S. (emelian@mail.utexas.edu).

PAI has shown tremendous potential in simultaneously providing structural, functional and molecular information in pre-clinical studies. PAI can visualize tumor location deep within a tissue, and is also able to provide information on tumor vasculature [4] or to monitor angiogenesis [5]. PAI can also obtain information on hemoglobin oxygen saturation at high resolution and contrast, without the use of exogenous contrast agents [4], which is a significant advantage when compared with other tumor hypoxia imaging techniques (e.g. blood oxygen level dependent-MRI and PET). Another advantage of PAI is compatibility with widely available USI techniques [6]; when combined, PAI and USI can simultaneously provide anatomical and functional information in tumors. For example, an *in vivo* study on human breast tissue has shown that an ultrasound image can depict the structure of ductal carcinoma, while photoacoustic (PA) images show the associated scattered distribution of vascularization [7].

With the availability of various targeted contrast agents, such as gold nanoparticles (AuNPs), several new avenues have opened up for *in vivo* molecular PAI. This has facilitated highly sensitive and specific detection of tumors. In addition, PAI, combined with other complementary imaging techniques, has shown promise in cancer treatment guidance. Although several reviews on the basics and applications of PAI are available, no examination of the recent developments in molecular PAI of cancer and the ability of PAI to monitor treatment is currently available; hence, we review these topics.

Basic principles of photoacoustic imaging

PAI (also known as optoacoustic imaging) capitalizes on the photoacoustic effect first described by Alexander Graham Bell in 1880 [8]. In this review, we provide only basic principles (Box 1) towards understanding PAI applicability to cancer detection and treatment guidance. Briefly, absorbed laser energy causes a rapid thermoelastic expansion of tissue, resulting in the generation of a wide-band ultrasound wave. The ultrasound wave is detected with a transducer that converts the mechanical acoustic waves to electric signals. The captured signals are then processed to form an image [6,9,10]. A typical PAI setup (Figure 1a) consists of two main components: a laser (generally a tunable, nanosecond pulsed laser) and a USI system. Most ultrasound image processing techniques translate directly to PAI. Delay and sum beamforming or more advanced computed tomography algorithms used in USI are also used in PAI to obtain images [10,11]. Other reviews have provided detailed information on equations governing the PA effect, various PA system configurations, and the image processing algorithms [6,9–12].

The contrast in PA images is largely determined by the wavelength-dependent μ_a (Equation I). The changes in optical absorption as a function of wavelength for a variety of endogenous chromophores, including melanin, oxy- (HbO_2) and deoxy-hemoglobin (Hb) are presented in Figure 1b. Because of the large variations in μ_a, spectroscopic or multi-wavelength imaging techniques are used for characterization of tumor tissue optical properties. For example, HbO_2 and Hb have different wavelength-dependent optical absorption properties, which allows spectroscopic PAI to differentiate between arteries and veins. Furthermore, HbO_2 and Hb have the same optical absorption at approximately 805 nm, PAI at this and other wavelengths can be used to assess total hemoglobin and blood oxygenation. PA contrast can also be enhanced by exogenous contrast agents (e.g. dyes or nanoparticles) (Figure 1c) that have distinct and tunable absorption spectra in the near-infrared (NIR) optical window (600–1100 nm) where endogenous chromophores, such as hemoglobin and water, have low absorption (Figure 1b).

Cancer detection with endogenous photoacoustic contrast

Cancer detection using PAI with endogenous chromophores (e.g. hemoglobin and melanin) is an area of active research. For example, PAI has been used to monitor melanoma tumor growth over the course of two weeks [23]. Optical contrast was provided by a higher concentration of melanin in the tumor relative to the surrounding tissue. PAI has also been used to detect skin melanoma [4,24]. Figure 2a depicts a melanoma and surrounding vasculature obtained by spectroscopic PAI. The pseudo-colored image was reconstructed from PA images obtained at 584 nm and 764 nm laser illumination. These studies indicate that PAI has the potential to identify, visualize, and track tumors and their associated vasculature with high resolution.

Malignant tumors have dense and unorganized vasculature compared to normal tissue. The high density of blood vessels in tumors enhances PA image contrast, thereby enabling tumor detection. For example, the Twente Photoacoustic Mammoscope was developed to detect breast carcinoma was based on this principle [21,25]. An X-ray mammogram (Figure 2b–i) and a sonogram (Figure 2b–ii) are compared with a PA image (Figure 2b–iii) obtained with a 1064 nm optical source. Figure 2 shows that the mammoscope is more sensitive to malignant indicators, such as vascularization, than conventional radiological techniques. PAI can also provide information on angiogenesis or changes in vasculature [5,26–28]. As shown in Figure 2c, sequential PA images can be obtained safely and noninvasively at different stages of tumor progression to monitor angiogenesis and to determine if a tumor has progressed to malignancy [5]. Compared to other vascular imaging techniques, including dynamic-enhanced MRI, CT perfusion, and functional PET [29], PAI detects tumor vasculature at a better or comparable resolution, without the use of exogenous contrast agents.

Besides imaging melanin and blood vessels, PAI systems have been employed for measuring the oxygen content of blood to study hypoxia in tumors [30,31]. Hypoxia is often linked to malignancy and resistance to therapy [32]. The amount of oxygen saturation in blood (SO_2) can be estimated by comparing the PA signal strength of HbO_2 and Hb obtained from spectroscopic PA images. Figure 2d shows *in vivo* functional imaging of a mouse brain with a glioblastoma. The blue hypoxic region (circled) indicates the location of the tumor in the brain [31]. The results clearly depict that the tumor has a lower percentage SO_2 than the surrounding normal tissue.

Metastatic spread of the primary tumor often leads to death in cancer patients. Highly sensitive detection of circulating tumor cells (CTCs) would greatly enhance overall patient survival, if treated. PAI has been used for detecting CTCs in the blood stream, with the goal of detecting metastasis. The label-free detection of CTCs *in vivo* in a blood vessel using PAI could provide higher detection sensitivity (~100-fold) compared to existing *ex vivo* CTC detection assays that use a small amount of blood. With the use of contrast agents targeted to CTCs, the PAI detection sensitivity can be enhanced further [33–35].

Cancer detection with exogenous photoacoustic contrast agents

The sensitivity of the PAI technique to image deeply situated tumors can be increased drastically by utilizing exogenous contrast agents. The NIR-absorbing dyes, such as IRDye800CW [31,36], AlexaFluor 750 [37] and indocyanine green (ICG) [38], have been used to enhance PA contrast. However, among the exogenous contrast agents, AuNPs have attracted attention in nanoparticle-based PAI owing to their unique optical properties from the surface plasmon resonance (SPR) effect. Because of the SPR effect, AuNPs have an absorbance that is orders of magnitude higher than NIR dyes. For example, gold nanospheres, nanorods, nanoshells, nanocages and nanobeacons have been used in PAI

because of their tunable and strong longitudinal plasmon resonance in the NIR [39–46]. The cytotoxicity of these nanoparticles is debatable and often emerges in a dose- and time-dependent manner for different types of nanoparticles; hence, further investigation into AuNPs toxicity is necessary [47]. The details on toxicity and pharmacodynamics of nanoparticles are beyond the scope of the review and are therefore not discussed here.

By attaching targeting moieties to exogenous agents, specific molecular information regarding the tumors can be obtained. AuNPs with different optical absorption properties can be conjugated to cancer-specific biomarkers, such as growth factor receptors and integrins (Table 1). By utilizing multiple targeted AuNPs, multiplex molecular labeling of a tumor can be achieved and multi-wavelength PAI can image the heterogenous accumulation and interaction of AuNPs with cancer cells *in vivo* [41]. Fluorescent optical probes, such as quantum dots, also provide PA contrast and can be used for multiplex labeling of tumors [48].

There have been several advances in molecular PAI that help describe crucial functional and molecular interactions between tumor cells and the surrounding micro-environment. For example, the feasibility of utilizing a multi-wavelength PAI technique to monitor molecular interactions of epithelial growth factor receptor (EGFR)-targeted AuNPs in 3D tissue cultures and *ex vivo* tissue has been evaluated [44,53]. Briefly, AuNPs (spheres of 50 nm diameter) functionalized with antibodies bind to EGFR. This specific targeting of AuNPs to EGFR causes plasmon resonance coupling between adjacent nanoparticles and changes their absorbance spectra so that it can be detected as a change in the PA signal amplitude. Overall, the results indicate that PAI together with bioconjugated AuNPs have the potential to image nano-molecular interactions. Because of the concerns that nano-scale agents might cause long-term toxicity *in vivo*, biodegradable gold nanoclusters have been developed as a contrast agent [54,55]. The size of these biodegradable nanoclusters, consisting of sub-5-nm AuNPs and a biodegradable polymer binder, is less than 100 nm. The nanoclusters are also pH-sensitive and will biodegrade in the acidic environment of the endosome. After degradation, the 5-nm AuNPs are excreted out of the body, thereby preventing toxic accumulations.

Another recent advancement in PAI is the use of photo-activable probes to provide a target-dependent photoacoustic signal and they show superior specificity and sensitivity as compared to the probes that donot interact with the target. For example, photo-activable probes have been designed to specifically target matrix metalloprotease 2 (MMP-2), a protease found to be overexpressed in many aggressive cancers[56]. The probe's peptide platform consists of an activatable cell-penetrating peptide (ACPP) that is recognizable by MMP-2, in both *in vitro* and mouse models. Before cleavage by MMP-2, the intact probe shows PA signals of similar intensity at the two wavelengths corresponding to the absorption maxima of the chromophores BHQ3 (675 nm) and AlexaFluor 750 (750 nm). When the probe is cleaved by the appropriate enzyme, the BHQ3 dye associated with the CPP portion of the probe accumulates in the nearby cells, while the Alexa dye diffuses away. This results in a PA signal visible only at 675 nm [56].

Recently, emphasis has been placed on multi-modal nanosystems that can enhance contrast in two or more imaging modalities, including microbubbles [57], perfluorocarbon-based nanobubbles [58], and nanowontons [59]. For example, nanowontons consist of ferromagnetic (cobalt core) core coated with gold for biocompatibility and a unique shape that enables optical absorption over a broad range of frequencies; the magnetic core acts as an MRI contrast agent and the gold coating provides the optical absorption contrast for PAI [59]. With the evolution of combined imaging strategies, these multi-modal nanostructures will play a prominent role in cancer detection and treatment.

Combination of PA with other imaging modalities

Assessing complementary structural, functional, metabolic and molecular information on a tumor with high accuracy is essential for cancer treatment. PAI primarily provides high-resolution images based on the optical contrast of tissue components, such as changes owing to abnormal vasculature or high melanin content; however, the overall anatomical structure of the tumor cannot be perceived by PAI alone. USI, a noninvasive technique when combined with PAI, can be used to obtain anatomical details about the tumor and its surrounding environment (Figure 3a). Both USI and PAI are highly synergistic: they utilize the same transducer and receiver electronics and are non-ionizing imaging modalities (unlike CT and PET) [6]. Indeed, commercial ultrasound systems have been modified to PAI systems for both small animal imaging and breast cancer imaging [12, 17, 60–63].

An imaging modality that can provide structural information at resolutions greater than ultrasound (~50–500 μm) is optical coherence tomography (OCT)(~10 μm), which relies on the optical backscattering properties of tissue. A 3D combined OCT and PA system has been constructed that can image microvasculature circulation (Figure 3b) [64]. This combined system could be used to image microvasculature of malignant skin lesions and provide comprehensive structural and functional information [65]. Other optical imaging modalities, such as fluorescence imaging (Figure 3c), have also been used with PAI to image brain tumors *in vivo* [31]. PAI provides high-resolution structural images of tumor angiogenesis, whereas fluorescence imaging has high sensitivity to molecular probes for detecting tumor location.

Ultrasound-based elasticity imaging non-invasively assesses the biomechanical properties (i.e. the Young's modulus) of tumors, which otherwise cannot be depicted from ultrasound or PA images (Figure 3d). A combination of ultrasound and elasticity imaging has shown the best results in detecting breast tumors *in vivo* with high sensitivity and specificity and could potentially reduce unnecessary biopsies [66]. A combination of complementary imaging techniques (e.g. elasticity coupled with USI and PAI) could further improve cancer detection sensitivity and specificity by providing simultaneous information on anatomy (USI), angiogenesis (PAI), and changes in mechanical properties (elasticity imaging) of the tumor [6]. Another ultrasound-based imaging technique that can be combined with PAI is magneto-motive USI (MMUS). MMUS has the potential to measure the biomechanical properties of the tissue with the aid of magnetic nanoparticles (Figure 3e) [67]. In MMUS, magnetic excitation is applied to induce motion of the magnetic nanoparticles within tissues or organs. Mechanical properties of tissue can be evaluated based on tissue motion detected in ultrasound images [68]. Based on the initial studies performed on tissue-mimicking phantoms, it can be predicted that the pathological changes in tissue, which are often related to changes in tissue mechanical properties, could be detected and differentiated using MMUS. However, further investigation in murine tumor models is required to evaluate the technique *in vivo*. With the recent introduction of *in vivo* imaging systems (e.g. Vevo 2100 by Visual Sonics Inc.) capable of both USI and PAI at microscopic or macroscopic resolution, the functional intricacies and the structural complexities of the tumor can be simultaneously visualized.

PAI for guiding, monitoring and evaluating therapy

Imaging techniques play a significant role in cancer therapy, from precise planning and guiding to evaluation of efficacy. In particular, PAI has shown potential in aiding therapies by providing sequential monitoring of tumor functional properties such as changes in tumor vasculature before, during, and after therapeutic procedures. The therapeutic agents used for photodynamic therapy (PDT)or photothermal therapy (PTT) can also act as PA contrast

agents owing to their high optical absorption properties in the NIR region (e.g., protoporphyrin IX for PDT and gold nanorods for PTT)[41,72].

PAI can assist in determining the location of the tumor, gauging the heterogeneities in vasculature within the tumor, and observing the heterogeneities in the therapeutic agent accumulation. For example, golden carbon nanotubes (GNTs) conjugated with an antibody specific to the lymphatic endothelial hyaluronan receptor-1 have been used to visualize heterogeneities of endogenous low-absorbing mesenteric structures in nude mouse (Figure 4a) [73]. The PA image provided information on heterogeneous accumulation of targeted GNTs (red regions in Figure 4a) to guide PTT to cause spatially specific thermal damage to the lymphatic walls [73]. In another study, PAI was performed to identify the location of a colon adenocarcinoma tumor. The tumor was then specifically ablated by high-intensity focused ultrasound (HIFU) with the guidance of PA images [74].

PAI has tremendous potential in guiding therapeutic procedures and could potentially provide oncologists structural and functional information regarding tumors to facilitate personalized therapy by customizing the therapy dose. In addition, PAI can also aid in customized delivery of drugs with use of multi-functional nanoparticles. An example of such a nanoagent is a silver nanosystem consisting of a poly(lactic-*co*-glycolic acid) (PLGA) polymer core and outer silver cage network. The outer silver cage enhances contrast in PAI and the inner core of the nanosystem contains the drug doxorubicin (Figure 4b). Initial studies indicated that the PLGA-based nanosystems have the potential to significantly increase contrast in PAI while delivering customized payloads of drug simultaneously to the tumor cells [75]. Another example for controlled and customized drug delivery is using light-triggered nano-constructs, such as microspheres containing the drug paclitaxcel encapsulated in hollow gold nanospheres (HAuNS). Depending on the concentration of HAuNS in the tumor, the light dose can be adjusted to allow sufficient release of drug paclitaxel [76]. In addition HAuNS can also act as a PTT agent. Very few *in vitro* studies are published illustrating these concepts and further investigations on *in vivo* tumor models are required for validation.

Monitoring functional or structural changes, such as changes in tumor tissue properties and variations in vascular destruction during therapeutic procedures is critical for prognosis and further treatment. Several *ex vivo* studies show the potential of PAI in monitoring therapeutic procedures. For example, it has been demonstrated using *ex vivo* liver tissue and chicken breast tissue that PAI is capable of sensitive detection of thermally-induced changes in tissue optical properties at depths of up to 30–50 mm with sub-millimeter resolution during thermal therapy [77,78]. In another study, PAI provided both high-resolution and high-tissue-contrast images to quantify changes in vessel morphology during PDT using protoporphyrin IX photosensitizer on a chicken chorioallantoic membrane tumor model [72].

In PTT, efficient optical absorbers, such as gold nanorods, are used to heat the tissue to higher temperatures causing thermal damage. For example, a tumor loaded with gold nanorods shows significant temperature elevations in response to laser irradiation (Figure 4c). Both PAI and USI can be used to obtain temperature maps of the tumor during PTT. Indeed, PA-based thermal imaging in the presence of strong optical absorbers has a higher signal-to-noise ratio when compared to USI-based thermal imaging [79]. The examples provided in this section clearly indicate the capability of PAI in guiding, customizing and monitoring therapeutic procedures.

Future outlook

Overall, PAI could become a valuable tool for cancer detection and diagnosis, tumor characterization, and treatment guidance. By differentiating the optical properties of tissues, PAI is well-suited to measure functional properties of tumors *in vivo*. For example, multi-wavelength PAI can visualize vasculature and identify hypoxic conditions of the tumors. Current functional imaging techniques suffer from poor spatial resolution or inadequate penetration depth. Conversely, PAI is non-ionizing and can image deep tissue structures with acceptable spatial resolution.

For functional cellular and molecular imaging *in vivo* at sufficient depths, contrast agent-mediated photoacoustics holds great promise. Various PA contrast agents ranging from plasmonic metal nanoparticles to FDA-approved dyes can be targeted to specific receptors in intact living tissue. Compared with endogenous contrast of tissue, PA contrast agents can be tuned to a specific wavelength to provide images with higher contrast and signal-to-noise ratio. As with any exogenous contrast agent, safety and biocompatibility of the agents must be further addressed.

PAI might also play an important role in several existing and emerging treatment modalities. PAI can image metal objects (e.g. needles, brachytherapy seeds, stents) and therefore guide therapeutic interventions [80]. The temperature-dependence of the PA signal can provide the thermal imaging of tissue needed for thermal therapeutic approaches. Exogenous contrast agents used for molecular PAI can also be multiplexed to function as drug delivery carriers activated internally or triggered remotely. Therefore, drug delivery and release is an active and expanding area of PAI.

Fundamentally, PAI can be performed in real-time. Real-time imaging is critical in many diagnostic and therapeutic applications of PAI. In deep-penetrating PAI, array-based ultrasound imaging probes are adopted, thus allowing real-time imaging of tissue where frame rate is primarily limited by the pulse repetition frequency of the laser. Therefore, from the instrumentation perspective, high repetition rate, high pulse energy, single-wavelength, or tunable pulsed laser sources designed for PAI are needed. From a clinical perspective, PAI combined with ultrasound could be easily implemented and adapted by clinicians familiar with ultrasonography. Biomedical photoacoustics have seen tremendous growth in the past two decades yet photoacoustic imaging is still in its infancy. Therefore, wide and rapid advancement of photoacoustics, ranging from instrumentation development to regulatory approvals to pre-clinical and clinical utility, is anticipated in the next decade.

Box 1: Principles of PAI

To describe the photoacoustic effect, a simplified Equation I, assuming 1D plane-wave propagation in a homogeneous medium, can be used:

$$p_0=\frac{\beta v_s^2}{C_p}\mu_a F_0 e^{-\mu_{eff} z}=\Gamma\mu_a F_0 e^{-\mu_{eff} z} \quad [I]$$

Where p_0 is the pressure rise immediately after thermo acoustic excitation in the photoabsorber; β is the thermal coefficient of volume expansion; v_s is the speed of sound in tissue; C_p is the specific heat capacity of the tissue at constant pressure; μ_a represents the optical absorption coefficient of the photoabsorber; F_0 is laser fluence at depth $z = 0$; Γ is the Gruneisen parameter or coefficient; and μ_{eff} is the effective extinction coefficient of the tissue, defined in Equation II as:

$$\mu_{eff} = \sqrt{3\mu_a(\mu_a + \mu_s')} \quad [II]$$

where μ_s is the scattering coefficient of tissue [6,9,10,13]. In practice, optical heterogeneities of the tissue and other effects can significantly complicte Equation I.

PAI spatial resolution is determined by overlap of optical and ultrasound beams [6,11,14]. For deep-penetrating PAI, the parameters of the ultrasound transducer are most critical: the axial resolution is inversely proportional to the transducer bandwidth (BW), and the lateral resolution is inversely proportional to the numerical aperture (NA) and center frequency of the transducer. Therefore, a transducer with high center frequency, high bandwidth, and large NA yields the best resolution images [6,11].

Penetration depth in PAI is limited by wavelength of laser illumination. Greater penetration depth can be achieved in the optical window (600–1100 nm) where tissue endogenous chromophores have less optical absorption. Imaging depths of up to 5–6 cm have been achieved [15–17] using radiant exposures below the maximum permissible exposure (MPE) imposed by the American National Standards Institute for human skin. The MPE limit at different wavelengths is 20 mJ/cm^2 at $400<\lambda<700$ nm; $20\times10^{0.002(\lambda-700)}$ mJ/cm^2 at $700<\lambda<1050$ nm; and 100 mJ/cm^2 at $1050<\lambda<1500$ nm [18].

There is a trade-off between imaging depth and resolution of PAI. As the imaging depth increases, frequency-dependent attenuation decreases the BW and center frequency of the ultrasound wave, resulting in poorer spatial resolution (Table I) [6]. Thus a number of PAI systems have been developed to image both microscopic or macroscopic features of tumors [9]. Photoacoustic microscopy systems sacrifice imaging depth to improve resolution to as low as 50 μm[4,6,19,20]. With a highly focused laser beam, a lateral resolution of 5 μm can be reached to image superficial capillaries [19]. Conversely, macroscopic PAI systems, with resolution on the order of hundreds of microns, are promising for tumor detection in deeper regions [15–17,21].

Acknowledgments

Partial support for this work provided by NIH under grants EB008101 and CA149740 is greatly acknowledged. The authors would also like to thank all researchers and scientists who contributed to the field of photoacoustics and, therefore, made this review paper possible.

References

1. Jemal A, et al. Cancer Statistics, 2010. CA Cancer J Clin. 2010; 60:277–300. [PubMed: 20610543]
2. Fass L. Imaging and cancer: a review. Mol Oncol. 2008; 2:115–152. [PubMed: 19383333]
3. Frangioni JV. New technologies for human cancer imaging. Journal of clinical oncology. 2008; 26:4012–4021. [PubMed: 18711192]
4. Zhang HF, et al. Functional photoacoustic microscopy for high-resolution and noninvasive in vivo imaging. Nat Biotech. 2006; 24:848–851.
5. Siphanto RI, et al. Serial noninvasive photoacoustic imaging of neovascularization in tumor angiogenesis. Opt. Express. 2005; 13:89–95. [PubMed: 19488331]
6. Emelianov SY, et al. Synergy and applications of combined ultrasound, elasticity, and photoacoustic imaging. IEEE International Ultrasonics Symposium. 2006:405–415.
7. Jose J, et al. Imaging of tumor vasculature using Twente photoacoustic systems. Journal of Biophotonics. 2009; 2:701–717. [PubMed: 19718681]
8. Bell AG. Upon the production of sound by radiant energy. American Journal of Science. 1880; 20:305–324.

9. Wang L. Multiscale photoacoustic microscopy and computed tomography. Nature Photonics. 2009; 3:503–509. [PubMed: 20161535]
10. Oraevsky, A.; Karabutov, A. Optoacoustic Tomography. In: Vo-Dinh, T., editor. Biomedical Photonics Handbook. CRC Press; 2003. p. 34/31-34/34.
11. Xu M, Lihong VW. Photoacoustic imaging in biomedicine. Review of Scientific Instruments. 2006; 77:041101.
12. Emelianov SY, et al. Photoacoustics for molecular imaging and therapy. Physics today. 2009; 62:34–39. [PubMed: 20523758]
13. Oraevsky AA, et al. Measurement of tissue optical properties by time-resolved detection of laser-induced transient stress. Appl. Opt. 1997; 36:402–415. [PubMed: 18250688]
14. Oraevsky AA, et al. Lateral and z-axial resolution in laser optoacoustic imaging with ultrasonic transducers. Proc. of SPIE. 1995; 2389:198–208.
15. Esenaliev RO, et al. Sensitivity of laser opto-acoustic imaging in detection of small deeply embedded tumors. IEEE Journal of Selected Topics in Quantum Electronics. 1999; 5:981–988.
16. Ku G, Wang LV. Deeply penetrating photoacoustic tomography in biological tissues enhancedwith an optical contrast agent. Opt. Lett. 2005; 30:507–509. [PubMed: 15789718]
17. Kim C, et al. Deeply penetrating in vivo photoacoustic imaging using a clinical ultrasound array system. Biomed. Opt. Express. 2009; 1:278–284. [PubMed: 21258465]
18. American National Standards Institute. "American National Standard for the Safe Use of Lasers", ANSI Z136.1-2000. New York: American National Standards Institute; 2000.
19. Maslov K, et al. Optical-resolution photoacoustic microscopy for in vivo imaging of single capillaries. Opt. Lett. 2008; 33:929–931. [PubMed: 18451942]
20. Mallidi S, et al. Functional and morphological ultrasonic biomicroscopy for tissue engineers. Proceedings of the SPIE Medical Imaging: Ultrasonic Imaging and Signal Processing. 2006; 6147 61470Y61471-61477.
21. Manohar S, et al. Initial results of in vivo non-invasive cancer imaging in the human breast using near-infrared photoacoustics. Opt. Express. 2007; 15:12277–12285. [PubMed: 19547596]
22. Prahl, SA. Optical property spectra compiled by Scott Prahl. 2001. http://omlc.ogi.edu/spectra/.)
23. Staley J, et al. Growth of melanoma brain tumors monitored by photoacoustic microscopy. Journal of Biomedical Optics. 2010; 15:040510–040513. [PubMed: 20799777]
24. Oh J-T, et al. Three-dimensional imaging of skin melanoma in vivo by dual-wavelength photoacoustic microscopy. Journal of Biomedical Optics. 2006; 11:034032–034034.
25. Manohar S, et al. The Twente Photoacoustic Mammoscope: system overview and performance. Physics in Medicine and Biology. 2005; 50:2543. [PubMed: 15901953]
26. Lao Y, et al. Noninvasive photoacoustic imaging of the developing vasculature during early tumor growth. Physics in Medicine and Biology. 2008; 53:4203. [PubMed: 18635896]
27. Kolkman, RGM., et al. Photoacoustic imaging of tumor angiogenesis; Photons Plus Ultrasound: Imaging and Sensing 2008: The Ninth Conference on Biomedical Thermoacoustics, Optoacoustics, and Acousto-optics; 2008. p. 685602-685606.
28. Ku G, et al. Imaging of tumor angiogenesis in rat brains in vivo by photoacoustic tomography. Appl. Opt. 2005; 44:770–775. [PubMed: 15751858]
29. Turkbey B, et al. Imaging of tumor angiogenesis: functional or targeted? American journal of roentgenology. 2009; 193:304–313. [PubMed: 19620425]
30. Lungu, et al. In vivo imaging and characterization of hypoxia-induced neovascularization and tumor invasion. 2006 Editorial Academy of the International Journal of Oncology.
31. Li M, et al. Simultaneous molecular and hypoxia imaging of brain tumors in vivo using spectroscopic photoacoustic tomography. IEEE International Ultrasonics Symposium. 2008; 96:481–489.
32. Hockel M, Vaupel P. Tumor hypoxia: definitions and current clinical, biologic, and molecular aspects. JNCI Journal of the National Cancer Institute. 2001
33. Zharov VP, et al. In vivo photoacoustic flow cytometry for monitoring of circulating single cancer cells and contrast agents. Opt. Lett. 2006; 31:3623–3625. [PubMed: 17130924]

34. Galanzha E, et al. In vivo, Noninvasive, Label-Free Detection and Eradication of Circulating Metastatic Melanoma Cells Using Two-Color Photoacoustic Flow Cytometry with a Diode Laser. Cancer Research. 2009; 69:7926–7934. [PubMed: 19826056]
35. Weight RM, et al. Photoacoustic detection of metastatic melanoma cells in the human circulatory system. Opt. Lett. 2006; 31:2998–3000. [PubMed: 17001379]
36. Stantz KM, et al. Molecular imaging of neutropilin-1 receptor using photoacoustic spectroscopy in breast tumors. Photons Plus Ultrasound: Imaging and Sensing. 2010:O1–O7.
37. Razansky D, et al. Multispectral photoacoustic imaging of fluorochromes in small animals. Optics letters. 2007; 32:2891–2893. [PubMed: 17909608]
38. Kim G, et al. Indocyanine-green-embedded PEBBLEs as a contrast agent for photoacoustic imaging. Journal of Biomedical Optics. 2007; 12:044020. [PubMed: 17867824]
39. Kim C, et al. In vivo molecular photoacoustic tomography of melanomas targeted by bioconjugated gold nanocages. ACS Nano. 2010; 4:4559–4564. [PubMed: 20731439]
40. Kim C, et al. In vivo photoacoustic tomography of chemicals: high-resolution functional and molecular optical imaging at new depths. Chemical reviews. 110:2756–2782. [PubMed: 20210338]
41. Li P, et al. In vivo photoacoustic molecular imaging with simultaneous multiple selective targeting using antibody-conjugated gold nanorods. Optics Express. 2008; 16:18605–18615. [PubMed: 19581946]
42. Agarwal A, et al. Targeted gold nanorod contrast agent for prostate cancer detection by photoacoustic imaging. Journal of Applied Physics. 2007; 102:064701–064704.
43. Li M, et al. In-vivo photoacoustic microscopy of nanoshell extravasation from solid tumor vasculature. Journal of Biomedical Optics. 2009; 14:0105071–0105073.
44. Mallidi S, et al. Molecular specific optoacoustic imaging with plasmonic nanoparticles. Optics Express. 2007; 15:6583–6588. [PubMed: 19546967]
45. Zhang Q, et al. Gold nanoparticles as a contrast agent for in-vivo tumor imaging with photoacoustic tomography. Nanotechnology. 2009; 20:395102. [PubMed: 19726840]
46. Pan D, et al. Molecular photoacoustic tomography with colloidal nanobeacons. Angewandte Chemie. 2009; 121:4234–4237.
47. Lewinski N, et al. Cytotoxicity of nanoparticles. Small (Weinheim an der Bergstrasse, Germany). 2008; 4:26–49.
48. Shashkov E, et al. Quantum dots as multimodal photoacoustic and photothermal contrast agents. Nano Letters. 2008; 8:3953–3958. [PubMed: 18834183]
49. De la Zerda A, et al. Ultrahigh Sensitivity Carbon Nanotube Agents for Photoacoustic Molecular Imaging in Living Mice. Nano Letters. 2010; 10:2168–2172. [PubMed: 20499887]
50. Homan K, et al. Prospects of molecular photoacoustic imaging at 1064 nm wavelength. Opt. Lett. 2010; 35:2663–2665. [PubMed: 20680092]
51. Xiang L, et al. Photoacoustic molecular imaging with antibody-functionalized single-walled carbon nanotubes for early diagnosis of tumor. Journal of Biomedical Optics. 2009; 14:021008. [PubMed: 19405721]
52. De La Zerda A, et al. Carbon nanotubes as photoacoustic molecular imaging agents in living mice. Nature Nanotechnology. 2008; 3:557–562.
53. Mallidi S, et al. Multiwavelength Photoacoustic Imaging and Plasmon Resonance Coupling of Gold Nanoparticles for Selective Detection of Cancer. Nano Letters. 2009; 9:2825–2831. [PubMed: 19572747]
54. Yoon SJ, et al. Utility of biodegradable plasmonic nanoclusters in photoacoustic imaging. Optics letters. 2010; 35:3751–3753. [PubMed: 21081985]
55. Tam JM, et al. Controlled assembly of biodegradable plasmonic nanoclusters for near-infrared imaging and therapeutic applications. ACS Nano. 2010; 4:2178–2184. [PubMed: 20373747]
56. Levi J, et al. Design, synthesis, and imaging of an activatable photoacoustic probe. Journal of the American Chemical Society. 2010; 132:11264–11269. [PubMed: 20698693]
57. Kim C, et al. Multifunctional microbubbles and nanobubbles for photoacoustic and ultrasound imaging. Journal of Biomedical Optics. 2010; 15:010510. [PubMed: 20210423]

58. Wilson K, et al. Synthesis of a dual contrast agent for ultrasound and photoacoustic imaging. Photons Plus Ultrasound: Imaging and Sensing. 2010:M1–M5.
59. Bouchard LS, et al. Picomolar sensitivity MRI and photoacoustic imaging of cobalt nanoparticles. Proceedings of the National Academy of Sciences of the United States of America. 2009; 106:4085–4089. [PubMed: 19251659]
60. Kolkman R, et al. Real-time in vivo photoacoustic and ultrasound imaging. Journal of Biomedical Optics. 2008; 13:050510. [PubMed: 19021380]
61. Niederhauser JJ, et al. Combined ultrasound and optoacoustic system for real-time high-contrast vascular imaging in vivo. IEEE Transactions on Medical Imaging. 2005; 24:436–440. [PubMed: 15822801]
62. Zemp RJ, et al. Photoacoustic imaging of the microvasculature with a high-frequency ultrasound array transducer. Journal of Biomedical Optics. 2007; 12:010501–010503. [PubMed: 17343475]
63. Jose J, et al. Imaging of tumor vasculature using Twente photoacoustic systems. Journal of Biophotonics. 2009; 2:701–717. [PubMed: 19718681]
64. Zhang EZ, et al. Multimodal simultaneous photoacoustic tomography, optical resolution microscopy, and OCT system. Photons Plus Ultrasound: Imaging and Sensing. 2010 75640U-75647.
65. Li L, et al. Three-dimensional combined photoacoustic and optical coherence microscopy for in vivo microcirculation studies. Optics Express. 2009; 17:16450–16455. [PubMed: 19770860]
66. Zhi H, et al. Comparison of ultrasound elastography, mammography, and sonography in the diagnosis of solid breast lesions. Journal of ultrasound in medicine : official journal of the American Institute of Ultrasound in Medicine. 2007; 26:807–815. [PubMed: 17526612]
67. Min Q, et al. Combined photoacoustic and magneto-acoustic imaging. IEEE Engineering in Medicine and Biology Society. 2009:4763–4766.
68. Mehrmohammadi M, et al. Pulsed Magnetomotive Ultrasound Imaging Using Ultrasmall Magnetic Nanoprobes. Molecular Imaging. 2010:1–11. [PubMed: 20128994]
69. Kim S, et al. Ultrasound and photoacoustic image-guided photothermal therapy using silica-coated gold nanorods: in-vivo study. Proceedings of the 2010 IEEE Ultrasonics Symposium. 2010 in press.
70. Wang L, et al. Combined photoacoustic and molecular fluorescence imaging in vivo. IEEE Engineering in Medicine and Biology Society. 2006:190–192.
71. Mallidi S, et al. Ultrasound-based imaging of nanoparticles: From molecular and cellular imaging to therapy guidance. IEEE International Ultrasonics Symposium. 2009:27–36.
72. Xiang L, et al. Real-time optoacoustic monitoring of vascular damage during photodynamic therapy treatment of tumor. Journal of Biomedical Optics. 2007; 12:014001. [PubMed: 17343476]
73. Kim J, et al. Golden carbon nanotubes as multimodal photoacoustic and photothermal high-contrast molecular agents. Nature Nanotechnology. 2009; 4:688–694.
74. Cui H, Yang X. In vivo imaging and treatment of solid tumor using integrated photoacoustic imaging and high intensity focused ultrasound system. Medical Physics. 2010; 37:4777–4781. [PubMed: 20964197]
75. Homan K, et al. Silver nanosystems for photoacoustic imaging and image-guided therapy. Journal of Biomedical Optics. 2010; 15:021316. [PubMed: 20459238]
76. You J, et al. Near-infrared light triggers release of Paclitaxel from biodegradable microspheres: photothermal effect and enhanced antitumor activity. Small. 2010; 6:1022–1031. [PubMed: 20394071]
77. Spirou GM, et al. Development and testing of an optoacoustic imaging system for monitoring and guiding prostate cancer therapies. Photons Plus Ultrasound: Imaging and Sensing. 2004
78. Larin K, et al. Monitoring of tissue coagulation during thermotherapy using optoacoustic technique. J. Phys. D: Appl. Phys. 2005; 38:2645.
79. Shah J, et al. Photoacoustic imaging and temperature measurement for photothermal cancer therapy. Journal of Biomedical Optics. 2008; 13:034024. [PubMed: 18601569]
80. Su J, et al. Photoacoustic imaging of clinical metal needles in tissue. Journal of Biomedical Optics. 2010; 15 021309-021306.

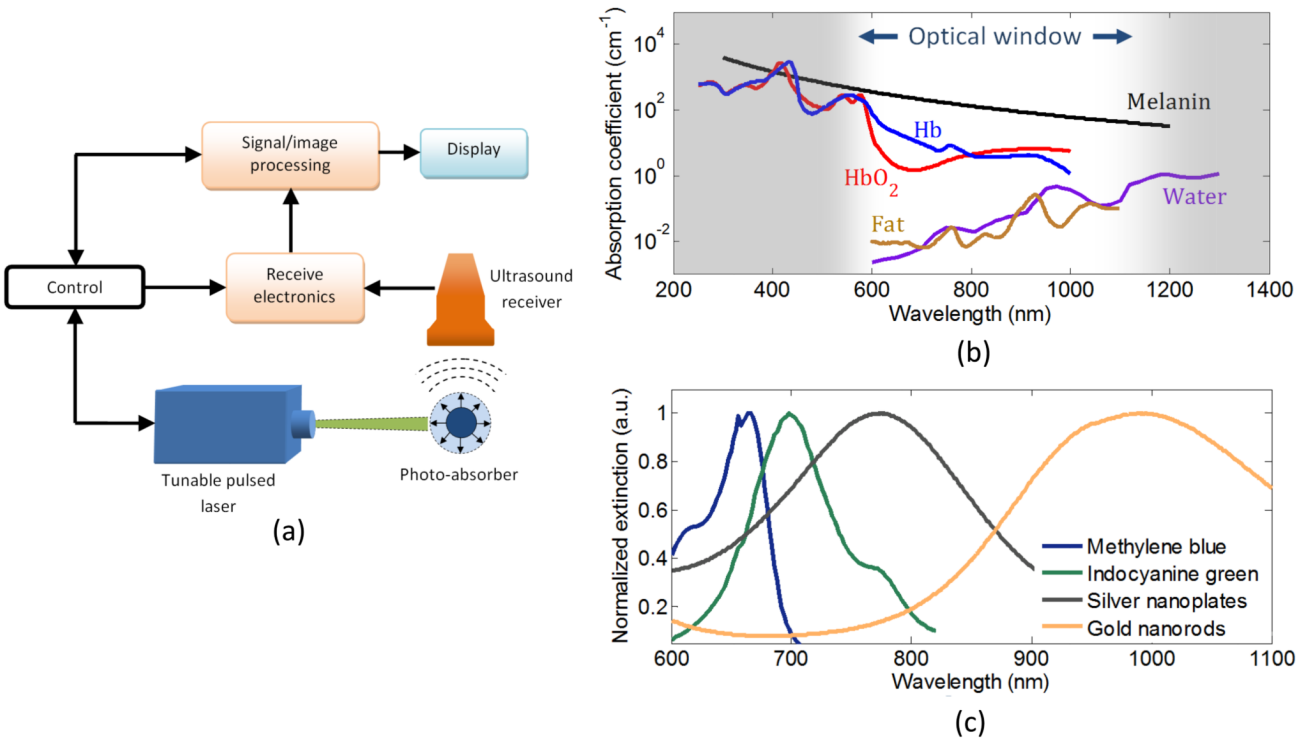

Figure 1.

(a) Block diagram of a typical PAI system. **(b)** Absorption spectra of endogenous chromophores in the body. The optical absorption of these endogenous chromophores is wavelength-dependent; therefore, PA signal intensity at different optical wavelengths can be used to characterize optical properties of tissue. Data for the absorption coefficient was obtained from [22]. The “optical window” (600–1100 nm) is the wavelength range where tissue absorption is at a minimum. **(c)** Extinction spectra of common exogenous contrast agents with peaks in the optical window.

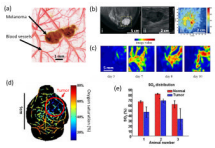

Figure 2.

(a) Overlaid maximum amplitude projections of PA images at 764 nm and 584 nm showing a tumor and its surrounding vasculature, respectively. The image clearly shows the vessel branching and structure around the tumor. Adapted with permission from [4]. **(b)** Images of the breast of 57 year old woman with invasive ductal carcinoma: **(i)** X-ray mammogram; **(ii)** sonogram; **(iii)** PA image at 1064 nm. The X-ray mammogram and the sonogram depict the gross anatomical features of the tumor, but donot provide functional information. The high PA amplitude corresponds to abundant vasculature associated with malignant tumors. The PA image clearly depicts that higher vascular densities are present in the tumor periphery and the core of the tumor has minimum vasculature. Adapted with permission from [21]. **(c)** Pancreatic tumor cells were inoculated on a rat hind leg on day 1. PAI was used to monitor angiogenesis associated with the tumor growth. PA images obtained from the tumor region on days 3, 7, 8 and 10 are maximum intensity projections of the photoacoustic source strength in the xy-plane (i.e. top view on the tumor tissue). Adapted with permission from [5]. **(d)** *In vivo* functional imaging of a mouse brain with a glioblastoma xenograft obtained using PAI. Spectroscopic PAI (wavelengths from 764 nm to 824 nm) was used to detect hypoxia in a braintumor. The heat map represents the percentage oxygen saturation (SO_2) in the blood vessels (blue = hypoxic; red = hyperoxic). The area indicated by the red arrow is the tumor. Adapted with permission from [31]. (e) A comparison of normal and brain tumor vasculature SO_2in three mice. Three normal vessels and three tumor vessels were chosen from each SO_2image that had been processed from spectroscopic PA images, such as the one shown in (d). The results clearly indicate that the percentage SO_2 in tumors is lower than the surrounding normal tissue, thus indicating hypoxia. Adapted with permission from [31].

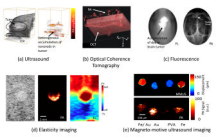

Figure 3.

Various optical- and ultrasound-based imaging techniques can be combined with PAI to provide structural, functional and biomechanical properties of the tissue. **(a)***In vivo* 3D USI and PAI of a subcutaneous tumor in a mouse injected with gold nanorods. The subcutaneous tumor appears as a bump in the 3D ultrasound image. The PA image shows the heterogenous localization of nanorods in tumor, which preferentially accumulate there owing to the enhanced permeation and retention effect [69]. **(b)***In vivo* PAI and OCT of the skin on the back of a nude mouse. The image represents a data fusion of OCT (structure of the skin) and PA (microvasculature) images. Adapted with permission from [64]. **(c)** Noninvasive *in vivo* fluorescence (FL) image acquired 24 hours after ICG injection in a mouse with melanoma cells implanted in brain. Noninvasive *in vivo* PA images were acquired with skin and skull intact, showing the vasculature in the brain. Adapted with permission from [70]. **(d)** Gray-scale ultrasound image (left), PA image (center), and elasticity (right) images of a tissue-mimicking phantom with a single inclusion. The inclusion had higher optical contrast and was harder compared to the background. **(e)** MMUS (top) and PA (bottom) images of a tissue-mimicking phantom with samples containing (left to right):a mixture of Fe_3O_4 nanoparticles and Au nanospheres; Au nanospheres only; PVA only (no nanoparticles); and Fe_3O_4 nanoparticles only. The MMUS colormap represents the displacement of the inclusions. The pure PVA sample (no nanoparticles) did not displace under magnetic excitation and showed no PA contrast. The Au nanospheres also do not displace, but have high optical absorption and hence produce greater PA signals compared with Fe_3O_4 nanoparticles. The two samples containing Fe_3O_4 nanoparticles had a displacement of about 100 μm [71].

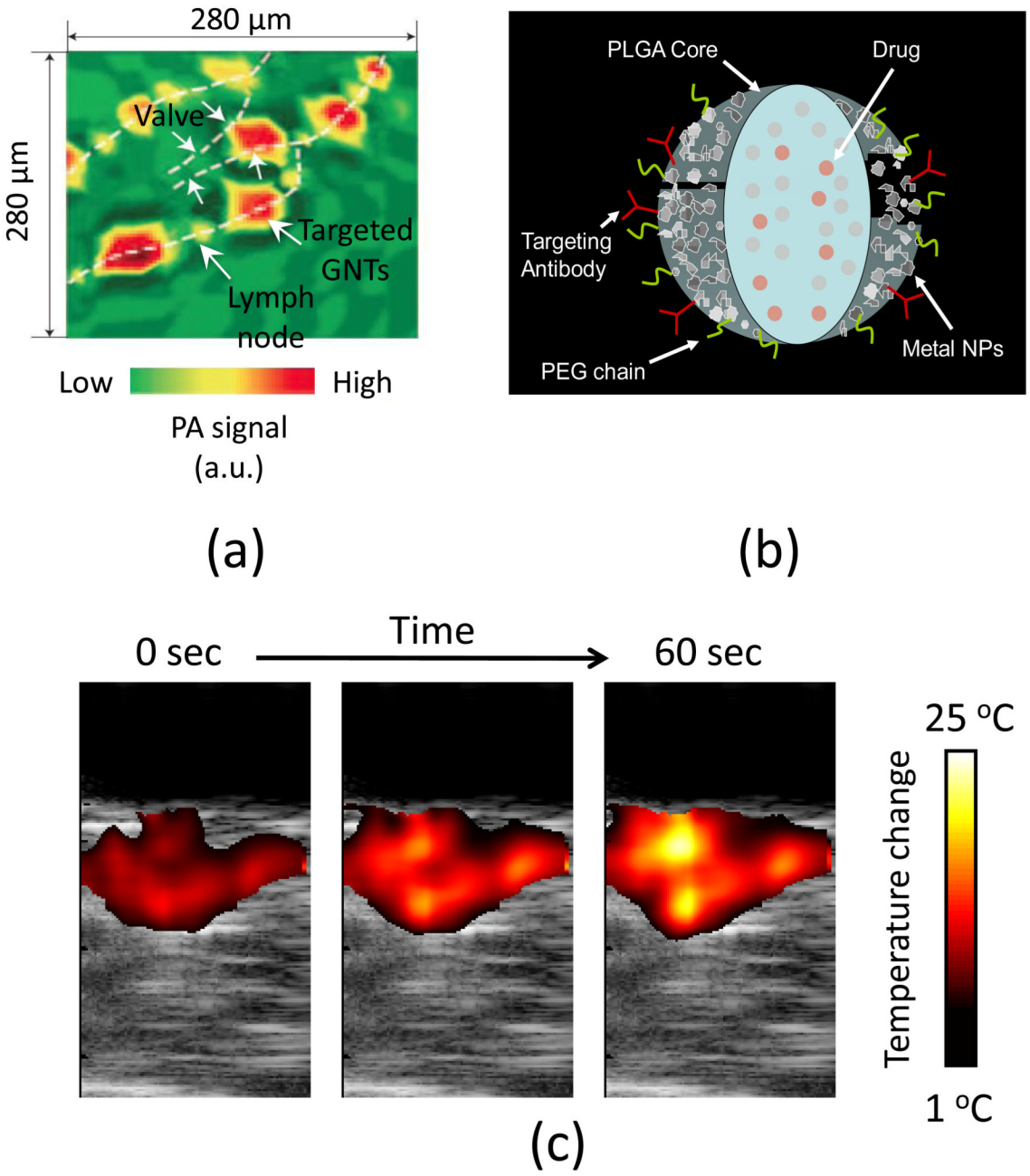

Figure 4.

(a) PAI can guide therapeutic procedures by providing an accurate biodistribution map of therapy agents. The white dotted lines represent the lymph node. The red regions indicate areas of higher accumulation of GNTs (i.e. in the lymph nodes). Therapeutic localization and dosage can be decided based on the guidance provided by the PA image regarding the location of GNTs. Adapted with permission from [73]. **(b)** Doxorubicin is encapsulated in the PLGA core, and the silver metal nanoparticles on the surface provide PA contrast for monitoring therapeutic response. Adapted with permission from [75]. **(c)** Therapeutic efficacy can be monitored in context of the anatomical map of the tumor tissue. USI and PAI can be used to monitor temperature increase during thermal therapy procedures. A mouse

was injected with optically absorbing gold nanorods that acted as both PA and photothermal agents. The tumor region was then irradiated with continuous-wave laser light at the peak absorption wavelength. Images taken after 0, 30 and 60 seconds of treatment indicate that the relative temperature rise in the tumor is 25 °C. Each image represents a 10.5 mm × 20 mm field of view.

Table I

Common USI and PAI imaging parameters

Parameter	Transducer frequency (MHz)	Axial resolution (μm)	Lateral resolution (μm)	Imaging depth (mm)
Ultrasound	5	150	300	70
Ultrasound	20	75	165	30
Macroscopic PAI	5	150	300	40
Microscopic PAI	50	15	50	3
Optical resolution PAI	75	15	5	0.7

Table 1

Exogenous PA contrast agents used for detecting tumors *in vivo*

Contrast agent	λ_{peak} (nm)	Tumor type	Target	Refs.
IRDye800[a]	800	Glioblastoma	Integrin $\alpha_v\beta_3$	[31]
IRDye800	800	Breast cancer	Neutropilin-1 receptor	[36]
Gold nanocages	778	Melanoma	Melanocyte-stimulating hormone	[39]
Gold nanorods	785 or 1000	Squamous cell carcinoma	HER2 and EGFR	[41]
Gold nanorods	810	Prostate cancer	HER2	[42]
Gold nanoshells	800	Colon carcinoma	None	[43]
Gold nanospheres	525	Breast cancer	None	[45]
Green-dye-enhanced single-walled carbon nanotube (SWNT-ICG)	780	Glioblastoma	Integrin $\alpha_v\beta_3$	[49]
Silver nanoplates	1064[b]	Pancreatic cancer	None	[50]
SWNT	750[c]	Glioblastoma	Integrin $\alpha_v\beta_3$	[51]
SWNT	690[c]	Glioblastoma	Integrin $\alpha_v\beta_3$	[52]

[a] IRDye800 (Li-Cor) was conjugated with a cyclic peptide that targets integrin $\alpha_V\beta 3$.

[b] λ_{peak} indicates the optical absorption peak of the nanoparticles and the wavelength at which PAI was performed.

[c] Nanoparticles such as carbon nanotubes do not have distinct optical absorption peaks in the optical window. For such nanoparticles, an optimum wavelength is chosen by the researchers to obtain PA image with enhanced contrast. In the table, the wavelength at which PAI was performed is considered the 'imaging' rather than the 'peak'λ.